ARTICLE   OPEN

Turning charge-density waves into Cooper pairs

Alla Chikina[1,2,5], Alexander Fedorov[1,3,5], Dilipkumar Bhoi[4], Vladimir Voroshnin[3], Erik Haubold[1], Yevhen Kushnirenko[1], Kee Hoon Kim[4] and Sergey Borisenko[1✉]

The relationship between charge-density waves (CDWs) and superconductivity is a long-standing debate. Often observed as neighbors in phase diagrams, it is still unclear whether they cooperate, compete, or simply coexist. Using angle-resolved photoemission spectroscopy, we demonstrate here that by tuning the energy position of the van Hove singularity in Pd-doped 2H-TaSe$_2$, one is able to suppress CDW and enhance superconductivity by more than an order of magnitude. We argue that it is particular fermiology of the material that is responsible for each phenomenon, thus explaining their persistent proximity as phases.

INTRODUCTION

Two, perhaps most fascinating ordering phenomena in solid-state physics, superconductivity and charge-density waves (CDWs), have a lot in common. Both are symmetry breaking phases characterized by an energy gap in a single-particle spectrum and a complex order parameter representing the existence of electron–electron or electron–hole pairs. In both cases, a re-organization of charge into waves or pairs needs a mediator, and thus requires a strong interaction between electrons and another degree of freedom, for example, lattice vibrations[1,2]. Both often have precursor phases above the critical temperature, characterized by, for example, pseudogap and Fermi surface arcs[3,4]. Finally, both are remarkably well explained by BCS (Bardeen–Cooper–Schrieffer) theory in their simplest manifestations—conventional superconductors and 1D Peierls systems, where phonons and fermiology (Fermi surface, underlying dispersion, the density of states at the Fermi level) play an essential role[5].

However, CDWs and superconductivity remain unexplained in more complicated cases, namely, in higher dimensions and high-T_C superconductors. Intriguingly, there both phases are often observed together, bordering in the generic phase diagrams. All hole-doped cuprates were found to exhibit CDWs[6–8] and archetypal CDW-bearing quasi-2D transition metal dichalcogenides (TMDs) 2H-NbSe$_2$ and 2H-TaSe$_2$ are superconductors[9,10]. While it is clear that the conventional BCS theory cannot explain the high-temperature superconductivity in the cuprates, the debates whether the Fermi surface nesting, explaining Peierls transition, is a requisite for CDW in 2D or not are ongoing[3,4,11–20].

The TMD's are very convenient systems to test whether the details of the electronic structure are important for the underlying mechanism of both phenomena, since the critical temperatures of both CDW and superconductivity are very different and can be relatively easily tuned. For example, crystallographically iso-structural 2H-NbSe$_2$ and 2H-TaSe$_2$ exhibit transitions to incommensurate CDW (iCDW) state at $T_{iCDW} = 33$ and 120 K, while the superconducting state is reached at $T_C = 7.3$ and 0.133 K[21,22], respectively, and the latter, in addition, enters a commensurate CDW (cCDW) state at $T_{CDW} = 90$ K. At the same time, the nesting of the Fermi surface in 2H-NbSe$_2$ was found to be weaker and a saddle-point singularity was found to be located below the chemical potential, contrary to 2H-TaSe$_2$, thus implying the crucial role of fermiology for both phenomena. Moreover, recent studies revealed that even moderate intercalation, application of pressure, or electron irradiation in one of the materials can lead to significant variation of the critical temperatures[23–26]. Since Pd intercalation induces more than an order of magnitude enhancement of T_C in 2H-Pd$_x$TaSe$_2$[23] and the electronic structure of the pristine material is well known[11–17,19,20], we initiated the present study to learn about the electronic structure of the Pd-intercalated one. Our measurements clearly identify a Lifshitz transition, which causes both destruction of nesting and shift of the van Hove singularity to the Fermi level, strongly implying that it is fermiology which plays an ultimate role in mechanisms of both ordering phenomena.

RESULTS

The electronic phase diagram of Pd-intercalated 2H-TaSe$_2$ is presented in Fig. 1a, as summarized in ref. [23]. With increasing Pd concentration, the cCDW phase is suppressed dramatically compared to the iCDW phase. At the same time, the superconducting $T_C(x)$ reveals a classic dome shape with an optimal T_C for $x = 0.08$–0.09. Notably, the collapse of cCDW phase coincides with the doping level where an optimal T_C is realized. In Fig. 1b, we have shown the temperature dependence of the in-plane resistivity, ρ_{ab}, of 2H-Pd$_x$TaSe$_2$ single crystal, close to the optimal Pd composition. For this composition, $\rho_{ab}(T)$ does not show any signature of the cCDW transition (inset of Fig. 1b). ρ_{ab} starts to drop near the onset temperature, $T_C^{on} \sim 3.29$ K and goes to zero at $T_C \sim 3$ K. Figure 1c shows the temperature dependence of the diamagnetic susceptibility, $4\pi\chi$, near the superconducting transition of the same crystal. The onset temperature of the diamagnetic susceptibility (~3 K) determined from the zero-field cooled susceptibility curve agrees well with $T_C \sim 3$ K, that is, zero resistivity temperature. At 1.9 K, $4\pi\chi$ reaches to 93%, indicating almost full Meissner shielding of the crystal used in the present study. Figure 1d displays the crystal structure and Brillouin zone of the 2H-TaSe$_2$.

Figure 1 implies that the CDW order hardly makes itself evident in the optimally intercalated samples. Neither resistivity nor

[1]IFW Dresden, P.O. Box 270116, 01171 Dresden, Germany. [2]Department of Physics and Astronomy, Interdisciplinary Nanoscience Center, Aarhus University, 8000 Aarhus C, Denmark. [3]Helmholtz-Zentrum Berlin für Materialien und Energie, Albert-Einstein-Strasse 15, 12489 Berlin, Germany. [4]Department of Physics and Astronomy, Center for Novel States of Complex Materials Research and Institute of Applied Physics, Seoul National University, Seoul 151-747, Republic of Korea. [5]These authors contributed equally: Alla Chikina, Alexander Fedorov. ✉email: s.borisenko@ifw-dresden.de
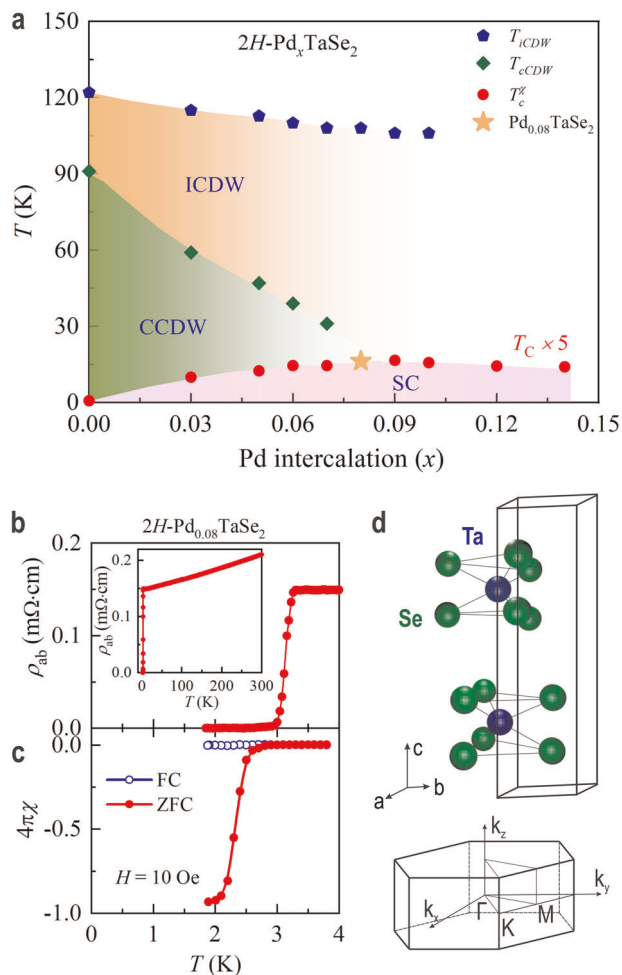
Fig. 1 Superconductivity and CDW in Pd-doped 2H-TaSe₂. a The electronic phase diagram of $2H\text{-}Pd_xTaSe_2$ as summarized in ref. [23]. The orange star represents $2H\text{-}Pd_{0.08}TaSe_2$, close to the optimal doping, used in the present investigation. For clarity the superconducting transition temperatures, $T_C(x)$, have been multiplied by a factor of 5. **b** Temperature dependence of resistivity of $2H\text{-}Pd_xTaSe_2$ ($x=0.08$) single crystal is presented below 4K and its inset shows the same in a wide temperature window below 300K. **c** Magnetic susceptibility after zero-field cooling (ZFC, filled) and field cooling (FC, open symbols) near the superconducting transition. **d** Crystal structure and sketch of the Brillouin zone (space group $P63/mmc$) of the 2H-TaSe₂.

susceptibility or specific heat curves show the signature of the transition. In the pristine material, in contrast, the resistivity curve clearly marked the transition to the iCDW state at around 120 K[23]. Remarkably, the only spectroscopic change at this temperature was the opening of the pseudogap[3] and no folding of the band structure occurred. Upon further lowering the temperature down to the commensurate lock-in transition, the replica of the bands started to appear and clear folding of the Fermi surface has been observed[3]. Interestingly, nearly no thermodynamic change has been seen in 2H-TaSe₂ across this second transition.

In order to identify the possible spectroscopic signatures of the CDW transitions in $2H\text{-}Pd_{0.08}TaSe_2$, we recorded its Fermi surface map and show the results in Fig. 2a. The first and most crucial observation is that the Fermi surface contour does not show any evidence for the CDW state, neither for the commensurate nor for the incommensurate one. At a first glance, similar to high-temperature Fermi surface of 2H-TaSe₂, it consists of hole-like pockets centered at the $\overline{\Gamma}$ and $\overline{K}$ points, and electron-like "dog-

bones" around the $\overline{M}$ point[15]. Earlier angle-resolved photoemission spectroscopy (ARPES) experiments have shown that the topology of 2H-TaSe₂ Fermi surface looks qualitatively similar in case of the high temperatures and the iCDW, while Fermi surface undergoes a 3×3 reconstruction at the cCDW state[3,4,16,20]. In the commensurate phase, the "heads" of the "dog-bones" around the $\overline{M}$ point are falling around the new 3×3 state $\overline{\Gamma}'$ point and rounded triangles form splitting the "dog-bones" on doubly degenerate concentric pockets around new $\overline{K}$ points. Here we do not see any of these changes. Also, no evidence for the pseudogap has been found in terms of spectral weight suppression or blurring of the parts of the Fermi surface. Therefore, we conclude that Pd doping suppresses all kinds of CDW order in optimally intercalated material.

The noticeable difference with the high-temperature Fermi surface of pristine sample[3] are the larger "dog-bones" and their apparent touching in the point lying on $\overline{\Gamma}$–$\overline{K}$ high-symmetry direction. This results in a closure of the second Fermi surface sheet around the $\overline{\Gamma}$ and $\overline{K}$ points seen in Fig. 2a, that is, a topological Lifshitz transition from a set of electron-like Fermi surfaces to two hole-like ones. In order to clarify this and reveal further fine details of the band structure of $2H\text{-}Pd_{0.08}TaSe_2$, we present in Fig. 2b–g the data taken along the principal **k** paths of the Brillouin zone indicated by numbers and dashed lines in Fig. 2a.

Intensity distribution along $\overline{\Gamma}$–$\overline{K}$ (crossing 1) clearly shows the presence of several features, not just two, in contrast to the pristine material. In the former, one has always detected an electron-like dispersion with two crossings of the Fermi level, corresponding to the hole pockets around $\overline{\Gamma}$ and $\overline{K}$ points, respectively. In the present case, there is an additional intensity in between these crossings. The second derivative plot (Fig. 2d) and corresponding EDC (Fig. 2e) unambiguously demonstrate that there are electronic states in the immediate vicinity of the Fermi level. The only possible origin of these states is the energy shifted saddle point singularity, which remained unoccupied in the unintercalated material[3]. The data along the $\overline{\Gamma}$–$\overline{M}$ direction (crossings 2 and 3) clearly support our earlier conclusion as regards the size of the "dog-bone" Fermi surfaces along this high-symmetry direction: unlike in pristine 2H-TaSe₂, Fermi momenta are very similar, indicating the very small separation between the big hole pocket around $\overline{\Gamma}$ and heads of the "dog-bones". This explains the much stronger intensity of the former in Fig. 2a. It actually consists now of two Fermi surfaces with similar sizes. Finally, the cut 4-4 shown in Fig. 2f and corresponding second derivative plot (Fig. 2g) confirm all our previous observations related to the Fermi surface topology. Indeed, the electronic states between points 4 are located slightly below the Fermi level. The hole-like character of this, perpendicular to $\overline{\Gamma}$–$\overline{K}$ direction dispersion manifests the presence of the van Hove singularity of the saddle-point type in $2H\text{-}Pd_{0.08}TaSe_2$ and this feature is now located at the Fermi level or slightly below it (see Supplementary Fig. 1a, b).

Figure 3 schematically summarizes our findings and compares the low-energy electronic structures of three key materials: high-temperature phase of 2H-TaSe₂, $2H\text{-}Pd_{0.08}TaSe_2$ and 2H-NbSe₂. As discussed above, in terms of the Fermi surface topology, we observe a gradual transformation of the electron-like "dog-bones" around $\overline{M}$ points into hole-like Fermi surface sheets around $\overline{\Gamma}$ and $\overline{K}$ points. The reason for this transformation is the change of the energetic location of the van Hove singularity from above the Fermi level in 2H-TaSe₂ to below it in 2H-NbSe₂, which is illustrated in the lower panels of Fig. 3 by dashed dispersion with red arrow. Remarkably, in optimally intercalated $2H\text{-}Pd_{0.08}TaSe_2$ its bottom nearly coincides with the Fermi level. We have also shown that this singularity is indeed a saddle point (not band edge), since along the cut perpendicular to $\overline{\Gamma K}$, the dispersion is hole like (see cut 4-4 in Fig. 2 and Supplementary Fig. 1). The presence of the singularities in the vicinity of the Fermi level seems to be a
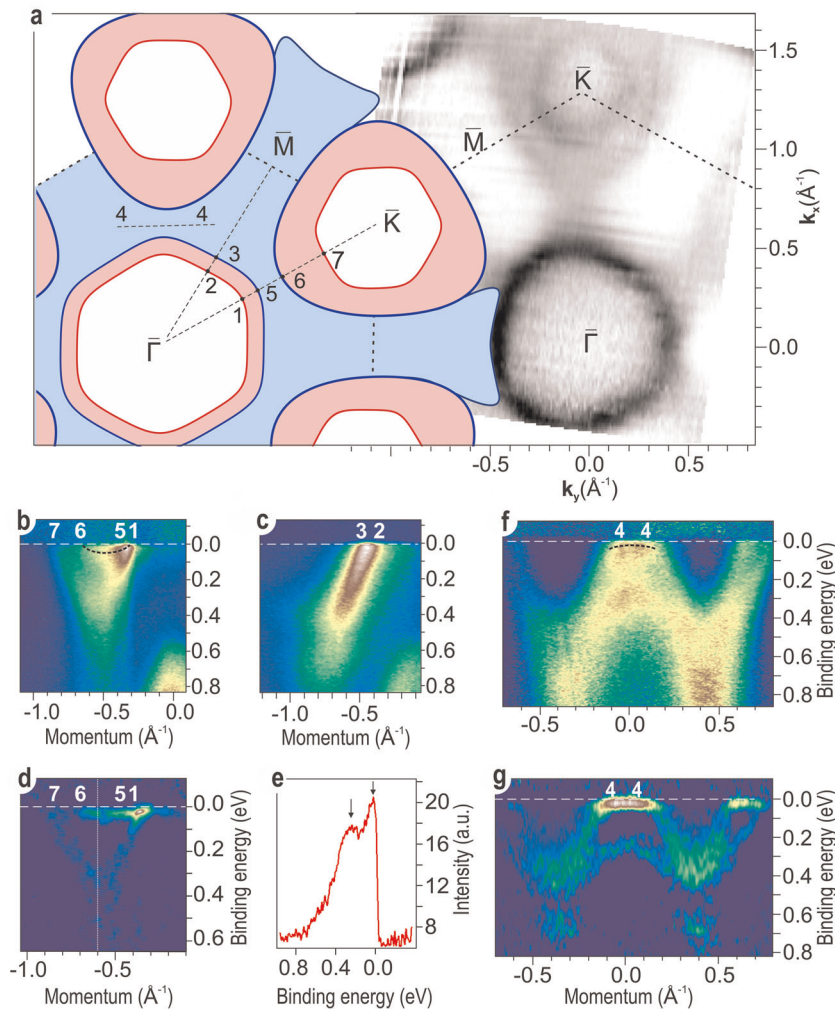
Fig. 2 Electronic band structure of 2H-Pd$_x$TaSe$_2$. a Fermi surface map taken at 80eV photon energy and a sketch of the Fermi surface pockets. **b**, **c**, **f** ARPES spectra along different momentum cuts in the BZ indicated in **a**. **d**, **g** Second derivative plots of intensity distributions from **b**, **f**, respectively. **e** EDC corresponding to the white vertical line in **d**.

necessary requisite for superconductivity (see Fig. 2 in ref. [27]). The reason is known from BCS theory[2]: the strength of the particular singularity defines the density of states, and thus is directly related to the critical temperature. Intriguingly, all higher-temperature superconductors are characterized by stronger than usual (e.g., logarithmic divergence due to saddle points in 2D systems) singularities. The examples are the cuprates having the extended saddle-point singularities[28] or iron-based superconductors having flat bands formed by multiband interactions (e.g., ref. [29], Fig. 4 in ref. [30], and ref. [31]). In this regard, we note the propensity to form an extended van Hove singularity in 2H-Pd$_{0.08}$TaSe$_2$ visible in Fig. 2d, g, implying that further tuning of the electronic structure may result in still higher critical temperatures in this system. On the other hand, in the Bi2201 cuprates it seems that the strong van Hove singularity may also result in iCDW order outside the pseudogap region[32].

Another result of our stuWelcome@123dy seen in Fig. 3 is the overall bandwidth renormalization of the band structure. While the bands in intercalated sample seem to just shift down, which is natural because of electron doping (and this is the driving mechanism behind the relocation of the singularity), comparison with 2H-NbSe$_2$ shows that the bandwidth is drastically different[33]. While the electronic structures of 2H-Pd$_{0.08}$TaSe$_2$ and 2H-NbSe$_2$ are qualitatively similar, the higher critical temperature in the latter may be explained either by higher density of states close to the

Fermi level, because of the overall stronger bandwidth renormalization or by better matching the energy of the pairing boson.

DISCUSSION

The evolution of the fermiology in mentioned dichalcogenides is in favor of nesting mechanism of CDW formation. A well known and very effective way to destroy the nesting is the shift of the chemical potential. Indeed, upon introducing additional charge carriers to the system, the sizes of $\bar{\Gamma}$- and $\bar{K}$-centered hole-like Fermi surface sheets decrease simultaneously, quickly increasing the distance between their sections responsible for very good nesting in pristine material (see Fig. 1 and Supplementary Fig. A in ref. [3]). The other sections of the Fermi surface overlapping upon the shift by CDW vector in 2H-TaSe$_2$ are the parts of the $\bar{K}$ barrel and electron-like "dog-bone." In this case, the distance between them decreases with electron doping destroying the nesting even more. As a result, we do not see any evidence for the CDW in this material. In 2H-NbSe$_2$, the change of the electronic structure is not due to doping and nesting is not destroyed completely. As a result, the CDW order survives only at significantly lower temperatures and remains incommensurate, making itself hardly visible spectroscopically[4]. We should point out that disorder induced by intercalated Pd atoms can be another reason for the suppression of CDW order in 2H-Pd$_{0.08}$TaSe$_2$[34]. At the same time,
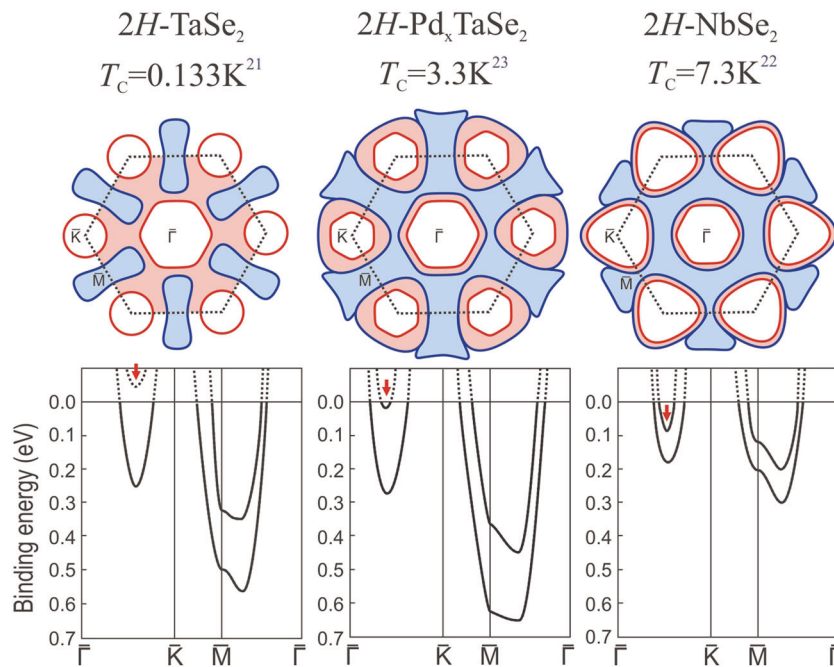
Fig. 3 Sketch of the electronic structure of 2H-TaSe$_2$, 2H-Pd$_{0.08}$TaSe$_2$, and 2H-NbSe$_2$. Upper row: Sketch of the normal state Fermi surfaces. Lower row: Corresponding band structures. The sketches are the summary of multiple measurements aimed to determine the peaks of the spectral function from raw ARPES data.

the alternative mechanism of CDW formation based on the nesting of saddle points[35] can most likely be ruled out: momentum separation of the unoccupied saddle points is very different from the CDW vectors in undoped case and even when they become occupied in the Pd-intercalated sample, CDW disappears.

Finally, our results shed more light on the coexistence of superconductivity and CDW in the phase diagrams. When the singularities are energetically close to the chemical potential, the resulting high density of states makes the system unstable with respect to the pairing. Already insignificant variation of the energy position of the singularity may quickly alter the electronic susceptibility, and thus nesting conditions because the Fermi velocities are very low. On the other hand, such variations may trigger the superconductivity, since the peaks of the density of states may reach the optimal position with respect to the Fermi level, for example, match with the low-energy boson. Obviously, the full picture of tuning the competition between the superconductivity and CDW should include the possible changes of such bosonic spectrum (e.g., phonons). Moreover, the role of the CDW fluctuations has to be clarified, since while the long-range ones definitely compete with superconductivity[36], their quantum version may favor superconductivity[37,38] and suppress long-range CDW order[39].

Our study is in line with the recent observation of the stress-driven Lifshitz transition in Sr$_2$RuO$_4$, where the uniaxial pressure resulted in lowering of the saddle-point singularity below the Fermi level, which caused enhancement of the superconducting critical temperature[40]. We speculate that the same mechanism is responsible for the strong T_C enhancement of 2H-TaSe$_2$ at high pressure[25].

Although the full understanding of high-T_C problem still requires a successful and comprehensive microscopic theory, we believe that the proximity of the van Hove singularities to the Fermi level is not only a necessary ingredient but also a crucial tuning parameter for controlling critical transition temperatures by pressure, strain, doping, intercalation, and so on.

METHODS

ARPES measurements were carried out at "1^3-ARPES" facility at BESSY at a temperature of 3 K within the range of photon energies (50–80 eV) from the cleaved surface of high-quality single crystals. The overall energy and momentum resolutions were set to ~8 meV and ~0.013 Å^{-1}, correspondingly. Polycrystalline samples of Pd$_x$TaSe$_2$ were synthesized via solid-state reaction method. Single crystal of the Pd$_x$TaSe$_2$ was grown by the chemical vapor transport method using SeCl$_4$ as a transport agent. Millimeter-sized hexagonal-shaped crystals were collected from the cold end of the quartz tube. The phase purity of the samples was determined by the powder x-ray diffraction using Cu Kα radiation at room temperature.

DATA AVAILABILITY

Data are available from the corresponding author upon reasonable request.

REFERENCES

1. Grüner, G. *Charge Density Waves in Solids* (Addison-Wesley Co., Advanced Book Program, 1994).
2. Bardeen, J., Cooper, L. N. & Schrieffer, J. R. Theory of superconductivity. *Phys. Rev.* **108**, 1175–1204 (1957).
3. Borisenko, S. V. et al. Pseudogap and charge density waves in two dimensions. *Phys. Rev. Lett.* **100**, 196402 (2008).
4. Borisenko, S. V. et al. Two energy gaps and Fermi-surface 'arcs' in NbSe$_2$. *Phys. Rev. Lett.* **102**, 166402 (2009).
5. Gabovich, A. M., Voitenko, A. I., Annett, J. F. & Ausloos, M. Charge- and spin-density-wave superconductors. *Supercond. Sci. Technol.* **14**, R1–R27 (2001).
6. Tranquada, J. M., Sternlieb, B. J., Axe, J. D., Nakamura, Y. & Uchida, S. Evidence for stripe correlations of spins and holes in copper oxide superconductors. *Nature* **375**, 561–563 (1995).
7. Ghiringhelli, G. et al. Long-range incommensurate charge fluctuations in (Y,Nd)Ba$_2$Cu$_3$O$_{6+x}$. *Science* **337**, 821–825 (2012).
8. da Silva Neto, E. H. et al. Ubiquitous interplay between charge ordering and high-temperature superconductivity in cuprates. *Science* **343**, 393–396 (2014).

9. Moncton, D. E., Axe, J. D. & DiSalvo, F. J. Study of superlattice formation in 2H-NbSe$_2$ and 2H-TaSe$_2$ by neutron scattering. *Phys. Rev. Lett.* **34**, 734–737 (1975).

10. Wilson, J. A., DiSalvo, F. J. & Mahajan, S. Charge-density waves in metallic, layered, transition-metal dichalcogenides. *Phys. Rev. Lett.* **32**, 882–885 (1974).

11. Liu, R., Tonjes, W. C., Greanya, V. A., Olson, C. G. & Frindt, R. F. Fermi surface of 2H-TaSe$_2$ and its relation to the charge-density wave. *Phys. Rev. B* **61**, 5212–5216 (2000).

12. Valla, T. et al. Charge-density-wave-induced modifications to the quasiparticle self-energy in 2H-TaSe$_2$. *Phys. Rev. Lett.* **85**, 4759–4762 (2000).

13. Rossnagel, K., Rotenberg, E., Koh, H., Smith, N. V. & Kipp, L. Fermi surface, charge-density-wave gap, and kinks in 2H-TaSe$_2$. *Phys. Rev. B* **72**, 121103 (2005).

14. Rossnagel, K. & Smith, N. V. Spin-orbit splitting, Fermi surface topology, and charge-density-wave gapping in 2H-TaSe$_2$. *Phys. Rev. B* **76**, 073102 (2007).

15. Inosov, D. S. et al. Fermi surface nesting in several transition metal dichalcogenides. *N. J. Phys.* **10**, 125027 (2008).

16. Rossnagel, K. On the origin of charge-density waves in select layered transition-metal dichalcogenides. *J. Phys.* **23**, 213001 (2011).

17. Laverock, J. et al. **k**-resolved susceptibility function of 2H-TaSe$_2$ from angle-resolved photoemission. *Phys. Rev. B* **88**, 035108 (2013).

18. Rahn, D. J. et al. Gaps and kinks in the electronic structure of the superconductor 2H-NbSe$_2$ from angle-resolved photoemission at 1 K. *Phys. Rev. B* **85**, 224532 (2012).

19. Ryu, H. et al. Persistent charge-density-wave order in single-layer TaSe$_2$. *Nano Lett.* **18**, 689–694 (2018).

20. Li, Y. W. et al. Folded superstructure and degeneracy-enhanced band gap in the weak-coupling charge density wave system 2H-TaSe$_2$. *Phys. Rev. B* **97**, 115118 (2018).

21. Kumakura, T., Tan, H., Handa, T., Morishita, M. & Fukuyama, H. Charge density waves and superconductivity in 2H-TaSe$_2$. *Czech. J. Phys.* **46**, 2611–2612 (1996).

22. Foner, S. & McNiff, E. J. Upper critical fields of layered superconducting NbSe$_2$ at low temperature. *Phys. Lett. A* **45**, 429–430 (1973).

23. Bhoi, D. et al. Interplay of charge density wave and multiband superconductivity in 2H-Pd$_x$TaSe$_2$. *Sci. Rep.* **6**, 24068 (2016).

24. Chatterjee, U. et al. Emergence of coherence in the charge-density wave state of 2H-NbSe$_2$. *Nat. Commun.* **6**, 6313 (2015).

25. Freitas, D. C. et al. Strong enhancement of superconductivity at high pressures within the charge-density-wave states of 2H-TaS$_2$ and 2H-TaSe$_2$. *Phys. Rev. B* **93**, 184512 (2016).

26. Cho, K. et al. Using controlled disorder to probe the interplay between charge order and superconductivity in NbSe$_2$. *Nat. Commun.* **9**, 2796 (2018).

27. Borisenko, S. Fewer atoms, more information. *Nat. Mater.* **12**, 600–601 (2013).

28. Abrikosov, A. A., Campuzano, J. C. & Gofron, K. Experimentally observed extended saddle point singularity in the energy spectrum of YBa$_2$Cu$_3$O$_{6.9}$ and YBa$_2$Cu$_4$O$_8$ and some of the consequences. *Phys. C* **14**, 73–79 (1993).

29. Charnukha, A. et al. High-temperature superconductivity from fine-tuning of Fermi-surface singularities in iron oxypnictides. *Sci. Rep.* **5**, 18273 (2015).

30. Maletz, J. et al. Photoemission and muon spin relaxation spectroscopy of the iron-based Rb$_{0.77}$Fe$_{1.61}$Se$_2$ superconductor: Crucial role of the cigar-shaped Fermi surface. *Phys. Rev. B* **88**, 134501 (2013).

31. Borisenko, S.V. et al. Strongly correlated superconductor with polytypic 3d dirac points. Preprint at https://arxiv.org/abs/1909.10806 (2019).

32. Peng, Y. Y. et al. Re-entrant charge order in overdoped (Bi,Pb)$_{2.12}$Sr$_{1.88}$CuO$_{6+\delta}$ outside the pseudogap regime. *Nat. Mater.* **17**, 697–702 (2018).

33. Borisenko, S. V. et al. Van Hove singularity as a possible origin of the bandwidth renormalization in layered superconductors. *J. Phys. Chem. Solids* **72**, 562–564 (2011).

34. Nie, L., Tarjus, G. & Kivelson, S. A. Quenched disorder and vestigial nematicity in the pseudogap regime of the cuprates. *Proc. Natl. Acad. Sci. USA* **111**, 7980–7985 (2014).

35. Rice, T. M. & Scott, G. K. New mechanism for a charge-density-wave instability. *Phys. Rev. Lett.* **35**, 120–123 (1975).

36. Arpaia, R. et al. Dynamical charge density fluctuations pervading the phase diagram of a Cu-based high-T$_c$ superconductor. *Science* **365**, 906–910 (2018).

37. Grissonnanche, G. et al. Direct measurement of the upper critical field in cuprate superconductors. *Nat. Commun.* **5**, 3580 (2014).

38. Caprara, S., Grilli, M., Lorenzana, J. & Leridon, B. Doping-dependent competition between superconductivity and polycrystalline charge density waves. *SciPost Phys.* **8**, 3 (2020).

39. Caprara, S., DiCastro, C., Seibold, G. & Grilli, M. Dynamical charge density waves rule the phase diagram of cuprates. *Phys. Rev. B* **95**, 224511 (2020).

40. Sunko, V. et al. Direct observation of a uniaxial stress-driven Lifshitz transition in Sr$_2$RuO$_4$. *npj Quant. Mater.* **4**, 46 (2019).

ACKNOWLEDGEMENTS

AUTHOR CONTRIBUTIONS

D.B. and K.H.K. provided and characterized high-quality single crystals. A.F., V.V., E.H., and Y.K. carried out ARPES experiments. A.C. analyzed the data. A.C. and S.B. formulated the message and wrote the paper.

COMPETING INTERESTS

The authors declare no competing interests.

ADDITIONAL INFORMATION

Supplementary information is available for this paper at https://doi.org/10.1038/s41535-020-0225-5.

Correspondence and requests for materials should be addressed to S.B.

Reprints and permission information is available at http://www.nature.com/reprints

Publisher's note Springer Nature remains neutral with regard to jurisdictional claims in published maps and institutional affiliations.